LAWRENCE
LIVERMORE
NATIONAL
LABORATORY

UCRL-TR-216920

Charge Carrier Density and signal induced in a CVD diamond detector from NIF DT neutrons, x-rays, and electrons

L. S. Dauffy, J. A. Koch

November 8, 2005

This work was performed under the auspices of the U.S. Department of Energy by University of California, Lawrence Livermore National Laboratory under Contract W-7405-Eng-48.

Charge Carrier Density and signal induced in a CVD diamond detector from NIF DT neutrons, x-rays, and electrons

Lucile S. Dauffy, Jeffrey A. Koch
Lawrence Livermore National Laboratory, Livermore, CA 94550
UCRL-TR-216920

Summary

This report investigates the use of x-rays and electrons to excite a CVD polycrystalline diamond detector during a double pulse experiment to levels corresponding to those expected during a successful (1D clean burn) and a typical failed ignition (2D fizzle) shot at the National Ignition Facility, NIF. The monitoring of a failed ignition shot is the main goal of the diagnostic, but nevertheless, the study of a successful ignition shot is also important. A first large neutron pulse is followed by a smaller pulse (a factor of 1000 smaller in intensity) after 50 to 300 ns. The charge carrier densities produced during a successful and failed ignition shot are about 10^{15} e-h+/cm^3 and $2.6*10^{12}$ e-h+/cm^3 respectively, which is lower than the 10^{16} e-h+/cm^3 needed to saturate the diamond wafer due to charge recombination. The charge carrier density and the signal induced in the diamond detector are calculated as a function of the incident x-ray and electron energy, flux, and detector dimensions. For available thicknesses of polycrystalline CVD diamond detectors (250 μm to 1000 μm), a flux of over 10^{11} x-rays/cm^2 (with x-ray energies varying from 6 keV to about 10 keV) or 10^9 β/cm^2 (corresponding to 400 pC per electron pulse, E_β > 800 keV) is necessary to excite the detector to sufficient levels to simulate a successful ignition's 14 MeV peak. Failed ignition levels would require lower fluxes, over 10^8 x-rays/cm^2 (6 to 10 keV) or 10^6 β/cm^2 (1 pC per electron pulse, E_β > 800 keV). The incident pulse must be delivered on the detector surface in several nanoseconds. The second pulse requires fluxes down by a factor of 1000.

Several possible x-ray beam facilities are investigated: (1) the LBNL Advanced Light Source, (2) the Stanford SLAC and SPEAR, (3) the BNL National Synchrotron Light Source, (4) the ANL Advanced Photon Source, (5) the LLNL Janus laser facility. None of the cyclotrons/synchrotrons (1) through (4) are bright enough. The maximum monoenergetic x-ray flux available at the energies of interest (6-10 keV) is about 10^4 x-rays/ns/cm^2 at 10 m from the source. The maximum white beam x-ray flux (thus all energies of x-rays are used) is about 10^6 x-rays/ns/cm^2 at 10 m from the source. These numbers are well below the necessary 10^{11} x-rays/cm^2 produced in a few ns. Also, producing double pulses separated from 50 to 300 ns with a factor of 1000 contrast between the first and second pulses seems very challenging using a cyclotron/synchrotron. The Janus laser-based x-ray facility (5) can generate over 10^{11} x-rays/cm^2 at 10 cm from the target (nickel or zinc target, 7.5 keV to 8.6 keV x-rays lines) and double pulses are possible.

Electron beams at the linac facility at LLNL can deliver from 5 to 100 pC double pulses, with electron energies varying from 15 to 90 MeV. Use of a 5 pC pulse could achieve the failed ignition densities, and a 100 pC pulse is just short of satisfying the densities of a successful ignition shot. Other linacs with higher current (400 pC per shot would be necessary) could satisfy both ignition densities.

A. Introduction

Characterization of a Deuterium-Tritium (DT) implosion during the ignition campaign at the National Ignition Facility (NIF) will rely on several diagnostics. Chemical Vapor Deposited (CVD) diamond is one of these diagnostics and it will measure the hot spot ion temperature and fuel areal density, ρR, along with the neutron flux. CVD diamond detectors are being tested to evaluate the feasibility of measuring ρR by determining the ratio of downscattered (~4-10 MeV) to primary (14 MeV) neutrons. The measurement of ρR remains a challenge because of the large dynamic range between the large 14 MeV peak and the downscattered neutron signal.

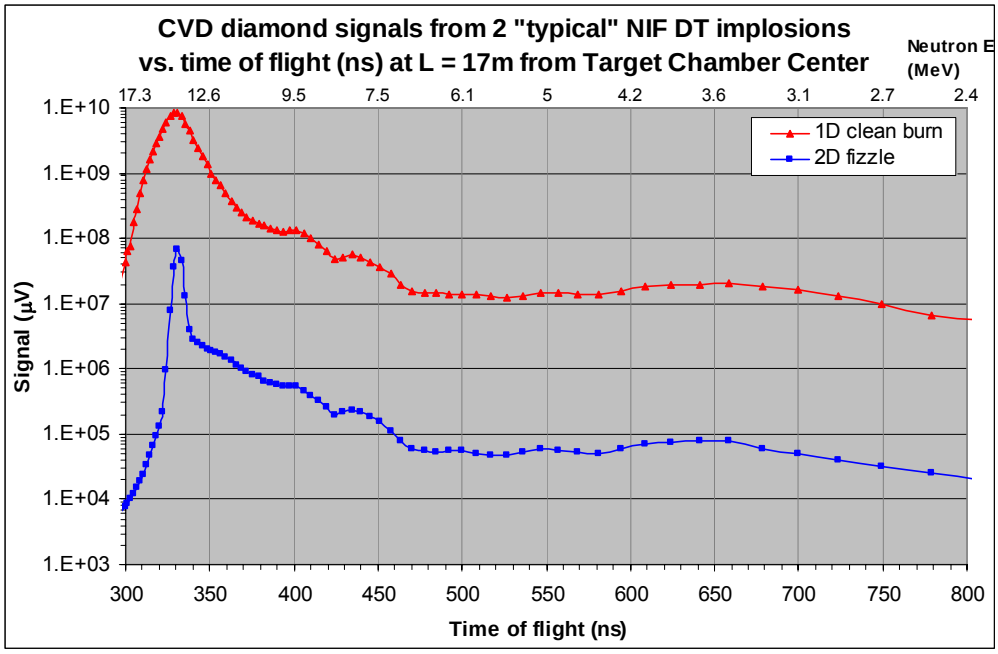

*Figure 1: Simulated neutron spectra recorded by a 1 cm^2 * 1 mm CVD diamond detector placed at 17 m from target chamber center. Two DT NIF implosions are simulated: 1D clean burn (success) and 2D fizzle (failure). Neutron/photon backgrounds, electronic noise, and electric field limitations are not included.*

Figure 1 shows an estimation of signals recorded by a 1 cm^2 * 1 mm CVD diamond during two different simulated DT shots: ignition success and failure.[1] These signals are not the ones observed on the oscilloscope, but are the signals corresponding to an idealized charge collected at the electrodes. This representation allows separating the charge created in the detector (figure 1), from the charge measured by the oscilloscope that is limited by the HV and the oscilloscope settings. The effects of the large 14 MeV peak on the downscattered signal must be understood and quantified before reliable ρR measurements can be made. Possible effects include saturation of the CVD diamond wafer, saturation of the biasing electronics, or/and saturation of the oscilloscope. Other sources of error in the ρR measurement include neutron-induced signals in the coaxial cable and uncertainty in the background.

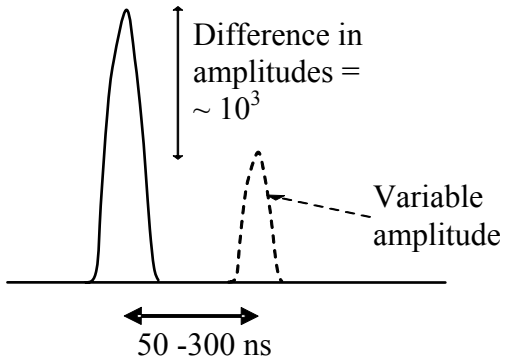

Figure 2: Idealized characteristics of the double pulse experiment

In order to imitate a large pulse followed by a smaller signal with an amplitude difference up to 1000, and a time delay of 50 to 300 ns (see figure 1), a double pulse experiment is being planned. A double pulse test was performed at the Bechtel Nevada facilities in Livermore in 2004[2], but we cannot draw adequate conclusions from this work, mainly because low energy photons were used (3.1 eV, which is lower than the 5.47 eV band gap energy[3,4] of diamond). Therefore, we are planning double pulse experiments using other kinds of radiation that can excite the diamond to appropriate levels, such as electrons or x-rays. The following report deals with the feasibility of using these radiations in a double pulse experiments with a first pulse that will resemble the 14 MeV neutron pulse of figure 1, and a second pulse that will have a lower amplitude, down by a factor of about 1000 (figure 2), and delayed by 50 to 300 ns. We specifically consider the saturation due to the creation of too many charge carriers in the detector's volume (carrier-carrier scattering), and the saturation due to the applied high voltage. Saturation due to the oscilloscope and part of the circuitry is being considered separately.

A few CVD diamond properties will be addressed in the next section to quantify the saturation from carrier-carrier scattering in the detector's volume and therefore verify if such a saturation occurs during a typical NIF DT implosion. Then equations for the calculation of the charge carrier density produced by incident x-rays and electrons will be presented, as well as the extraction of this quantity from figure 1 for both failed and successful ignition. The x-ray and electron fluxes and energies that are required to reach NIF implosion charge carrier densities will be calculated. Finally, x-ray and electron beam facilities will be reviewed to check if the necessary requirements can be met.

B. CVD diamond detector properties

B.1. Charge carrier density and saturation of a CVD diamond detector due to the decrease in charge carrier mobility (carrier-carrier scattering)

When a incident particle or wave goes through a diamond wafer, it ionizes a part of the volume by creating electron-hole pairs (charge carriers). The charge carrier density, $D_{e-/h+}$, is the number of electron-hole pairs created, $N_{e-/h+}$, per unit volume of the

detector, and has units of $N_{e-/h+}/cm^3$. The number of electron-hole pairs created is a function of the ionization energy of the diamond crystal and the energy deposited.[5-7] The ionization energy is noted $\varepsilon_{e-/h+}$, and is the average energy expended by a charged particle or photon to produce one electron-hole pair. $\varepsilon_{e-/h+}$ varies from about 13 eV/e^-h^+ (13-13.6 reported by the majority of researchers[8-10]) to 16.1 eV/e^-h^+ (reported by Kaneko and al.[11]) for both natural and CVD diamonds. An average value of 13.3 eV/e^-h^+ is used in this work. The energy absorbed in the crystal is converted into both ionization energy (creation of electron-hole pairs) and phonons (lattice vibrations), so that the energy it takes to create an electron-hole pair is always larger than the bandgap energy, by a factor of about 3.[7,12,13] The number of electron-hole pairs created, $N_{e-/h+}$, and the induced charge created in the detector's volume, Q_{dep} (C), are then:

$$N_{e^-/h} = \frac{E_{dep}(eV)}{\varepsilon_{e^-/h^+}} \quad (1)$$

$$Q_{dep} = 1.6*10^{-19} * N_{e^-/h} \quad (2)$$

The saturation of a semiconductor can be defined as a change in the charge collection distance as a function of the charge carrier density. The charge collection distance, d, is the mean separation of the electron and hole before they become trapped in the material, and is the common quantity to define the quality of a semiconductor.[14] When d is larger or equal to the thickness of the detector, ℓ, then 100% of the charges created will reach the electrodes. When d is smaller than ℓ, then only a fraction of the charges created will reach the electrodes. This fraction is called the efficiency of the detector, η, and is equal to the ratio of d over ℓ. The expression of d is given in the following equation[4,15,16]:

$$d = (\mu_e \tau_e + \mu_h \tau_h)E \quad (3)$$

where d is in cm, μ_e and μ_h are respectively the electron and hole mobilities in cm^2/Vs, τ_e and τ_h are the electron and hole lifetimes in s, and E is the electric field through the wafer in V/cm. It is often convenient to treat the conduction with a single-carrier model where mobilities and lifetimes are not differentiated for holes and electrons:

$$d = \mu\tau E \quad (4)$$
$$\mu\tau = \mu_e \tau_e + \mu_h \tau_h$$

For a fixed electric field, d is then a function of μ and τ. The saturation of the semiconductor volume, in number of charges created, will consequently occur when μ and τ vary. Several studies have been done on the variation of mobilities and lifetime of charge carriers in natural and CVD diamonds.[4,16-18] They find that the lifetime goes up slowly for a charge carrier density $D_{e-/h+}$ greater than 10^{16} e^-h^+/cm^3, whereas the mobility goes down sharply above 10^{16} e^-h^+/cm^3, reaching a slope of $\mu \approx 1/D_{e-/h+}$ after $2*10^{17}$ e^-h^+/cm^3. A typical low-density value of 500 ps for τ and 4000 cm^2/Vs for μ are used in this report,[4,17] corresponding to a $\mu\tau$ product of $2*10^{-6}$ cm^2/V, a value similar to that

noted in other studies.[19-21] The low-density charge collection distance is then 200 µm at 1 V/ µm. This value of d differs depending on the quality of diamonds: d is about 200 to 300 µm for a polycrystalline CVD diamond,[9,19] from 420 µm[19] to 20 cm[20,22] for single crystal CVD diamond, and less than 100 µm for a natural diamond[16]. The value 200 µm at 1 V/µm will be used in this work, 1 V/µm being a typical value of the electric field through a CVD diamond wafer.

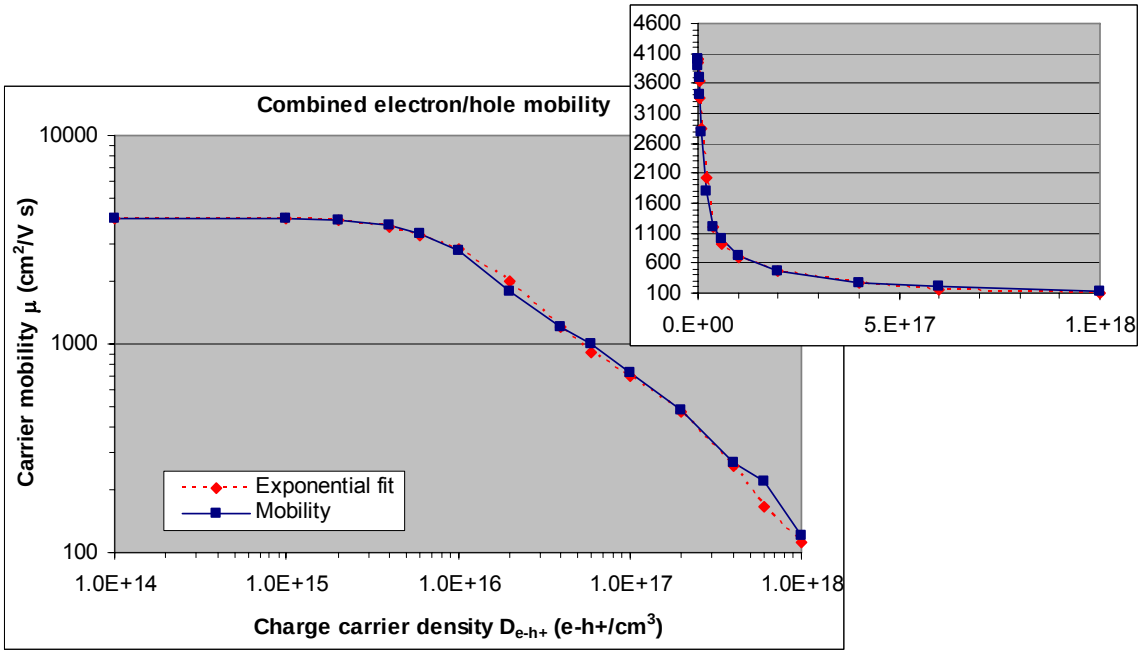

Figure 3. Combined electron/hole mobility, µ, as a function of the charge carrier density, $D_{e-/h+}$.[4,16-18] *The dashed line is a exponential fit to the curve. The upper right graph is a linear-linear plot.*

The mobility data found in the studies previously mentioned[4,16-18] is plotted in figure 3, and an exponential fit is added. The equation of the fit is given by the following data where µ is in units of cm^2/Vs:

$$\mu(D_{e^-/h^+}) = 4000 \qquad \text{when } D_{e^-/h^+} \le 2E+15$$

$$\mu(D_{e^-/h^+}) = \Delta + A_1 * e^{-D_{e^-/h^+}/\delta_1} + A_2 * e^{-D_{e^-/h^+}/\delta_2} \qquad \text{when } D_{e^-/h^+} > 2E+15$$

where $A_1 = 3300$, $\delta_1 = 1.8E+16$, $A_2 = 900$, $\delta_2 = 2.3E+17$, $\Delta = 100$. We can then calculate d for a certain value of the electric field using the values of µ and τ (equation 4). A figure showing the variation of τ is omitted because the increase of τ versus $D_{e-/h+}$ is negligible compared to the decrease of µ. Figure 4 gives d as a function of $D_{e-/h+}$ for a typical electric field of 1 V/µm, where the exponential fit is given by (d is in µm):

$$d(D_{e^-/h^+}) = 200 \qquad \text{when } D_{e^-/h^+} \le 2E+15$$

$$d(D_{e^-/h^+}) = \Delta + A_3 * e^{-D_{e^-/h^+}/\delta_3} + A_4 * e^{-D_{e^-/h^+}/\delta_4} \qquad \text{when } D_{e^-/h^+} > 2E+15$$

where A_3 = 150, δ_3 = 1.8E+16, A_4 = 50, δ_4 = 2.7E+17, Δ = 14. Therefore, for a charge carrier density above about 10^{16} $e^-/h^+/cm^3$, we estimate that there will be saturation of the CVD diamond detector, i.e. the wafer does not respond linearly. That does not take into consideration the saturation due to the high voltage supply or the detection electronics.

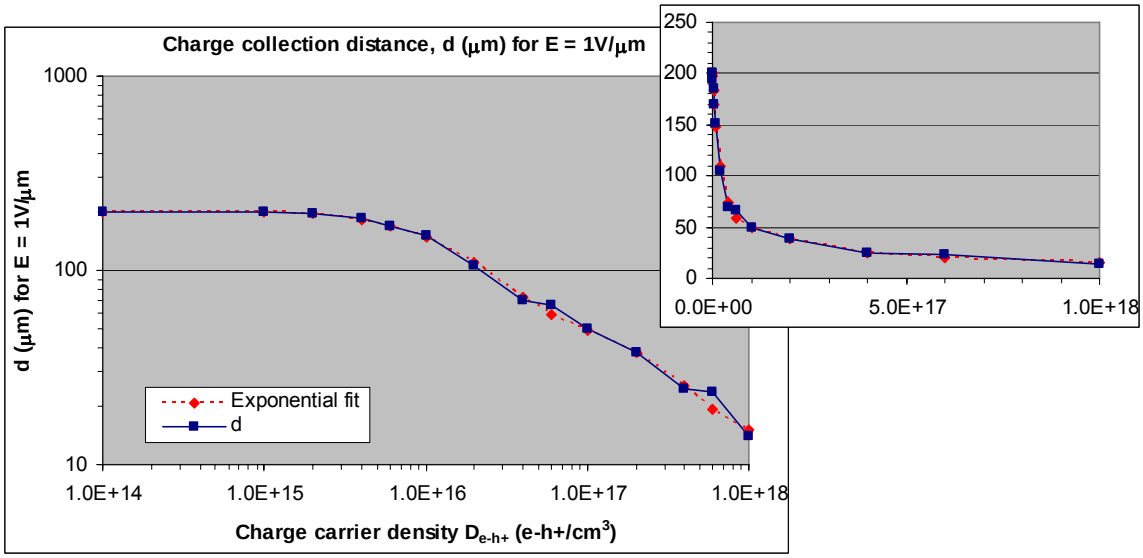

Figure 4. Charge collection distance, d, as a function of the charge carrier density, D_{e^-/h^+}. The dashed line is a exponential fit to the curve. The upper right graph is a linear-linear plot.

B.2. Efficiency and sensitivity of a CVD diamond detector

Before calculating the charge carrier density and signal produced in the CVD diamond detector volume by an incident particle or wave, one has to define the efficiency and sensitivity of the detector. The sensitivity of a detector, ζ, is given by the following equation:

$$\zeta = \frac{Q_{meas}(C)}{E_{dep}(J)} = \underbrace{\frac{Q_{meas}(C)}{Q_{dep}(C)}}_{\eta} * \underbrace{\frac{Q_{dep}(C)}{E_{dep}(J)}}_{\zeta_{int}} \qquad (5)$$

where the sensitivity is in units of coulombs of charge measured at the electrodes per joule of deposited energy in the detector's volume. The term Q_{meas} is the charge collected at the electrodes, Q_{dep} and E_{dep} are respectively the ionization charge produced and the energy deposited by the incident particles.

The efficiency of the detector, η, is defined as follow:[23,24]

$$\eta = \frac{Q_{meas}}{Q_{dep}} = \frac{d}{\ell} = \frac{\mu\tau E}{\ell} \qquad (6)$$

where d is the charge collection distance and ℓ is the detector thickness having the same unit as d. In this equation and in all the following equations, the maximum value of d is ℓ, since the distance traveled by the charges will never exceed ℓ (thus the maximum value for η is 1). The value of the efficiency will increase with the electric field until reaching a constant value. For a typical operation of the detector, i.e. below saturation of the wafer due to decrease in mobility and below electric fields of 4 V/μm[25], the efficiency remains constant. Equation 6 shows that the efficiency is a function of d, thus outside these typical operations, η will drop for $D_{e\text{-}h+}$ larger than 10^{16} $e^{-}h^{+}/cm^{3}$ and for E larger than 4 V/μm.

The intrinsic sensitivity of the diamond, ζ_{int}, is given by the following equation:

$$\zeta_{int}\left(\frac{C}{J}\right) = \frac{Q_{dep}}{E_{dep}} = \frac{1}{\varepsilon_{e^{-}/h^{+}}} = 7.52 * 10^{-2} \qquad (7)$$

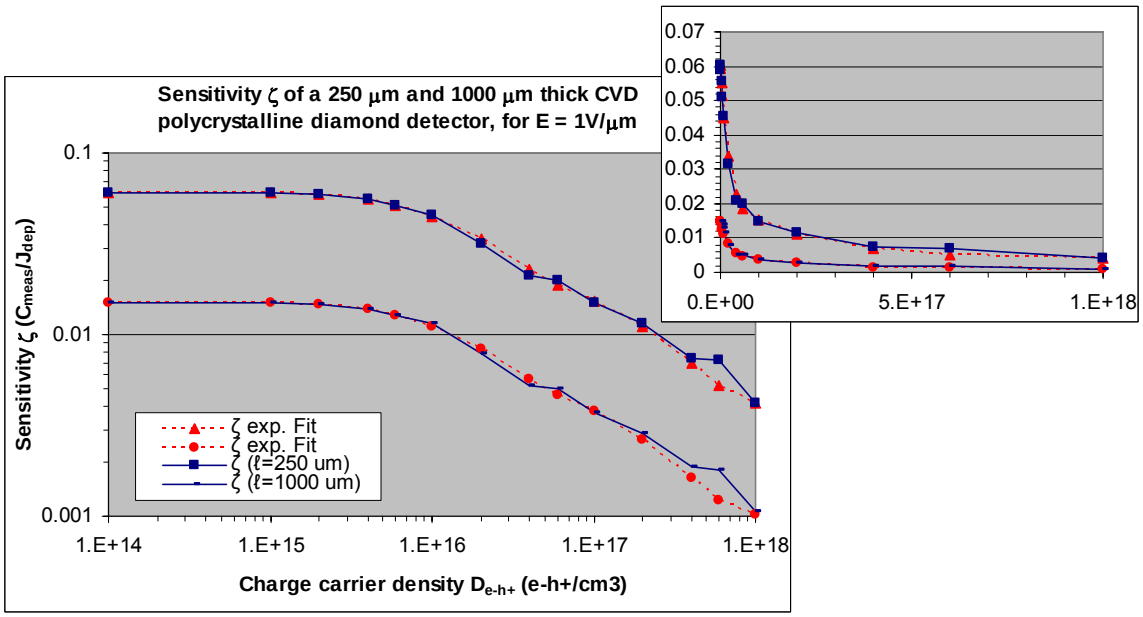

Figure 5. Sensitivity, ζ, in units of measured coulombs per deposited joules as a function of the charge carrier density, $D_{e\text{-}/h+}$. The dashed line is an exponential fit to the curve.

The sensitivity of a CVD detector will then be:

$$\zeta\left(\frac{C}{J}\right) = \frac{\eta}{\varepsilon_{e^-/h^+}} = \frac{d}{\ell\ \varepsilon_{e^-/h^+}} = \frac{\mu\tau E}{\ell\ \varepsilon_{e^-/h^+}} \tag{8}$$

where the ionization energy, $\varepsilon_{e\text{-}/h+}$, is in units of eV/e^-h^+. As previously mentioned, if the value of d is larger than ℓ, then ζ will be equal to $1/\varepsilon_{e\text{-}/h+}$. The dimensions of the detector are set by the manufacturer. Thicknesses vary from 250 to 1000 μm, and diameters go up to several inches for polycrystalline CVD diamonds.[26] Figure 5 gives the sensitivity of a 250 and 1000 μm polycrystalline CVD diamond as a function of $D_{e\text{-}h+}$, for E = 1 V/μm. The dashed lines are an exponential fit to the sensitivity. The equation of the fit is:

$$\zeta(D_{e^-/h^+}) = \Delta + A_5 * e^{-D_{e^-/h^+}/\delta_5} + A_6 * e^{-D_{e^-/h^+}/\delta_6}$$

where for the 250 μm CVD: $A_5 = 0.043$, $\delta_5 = 1.8E{+}16$, $A_6 = 0.017$, $\delta_6 = 2.3E{+}17$, $\Delta = 0.004$, and for the 1000 μm CVD: $A_5 = 0.0105$, $\delta_5 = 1.7E{+}16$, $A_6 = 0.0045$, $\delta_6 = 2.0E{+}17$, $\Delta = 0.001$. Table 1 gives values of the efficiency, intrinsic sensitivity, and sensitivity as a function of the CVD diamond detector thickness.

Table 1. Efficiency, η (unitless), sensitivity (mC/J) of a polycrystalline CVD diamond detector wafer versus its thickness, ℓ (μm). The charge collection distance, d, is equal to 200 μm at E=1V/μm and the intrinsic sensitivity, ζ_{int} is equal to 75.2 mC/J.

ℓ	250	300	400	500	600	700	800	900	1000
Efficiency	0.80	0.67	0.50	0.40	0.33	0.29	0.25	0.22	0.20
Sensitivity	60.2	50.1	37.6	30.1	25.1	21.5	18.8	16.7	15.0

C. Induced signals from x-rays, electrons, and DT neutrons

Radiation, incident on the surface of the detector as seen on figure 6, induces a signal by creating electron/holes in the wafer, which are collected by the electrodes. Typical electrodes for CVD diamonds used at LLNL and at the Laboratory for Laser Energetics (LLE, Rochester, New York) are made of 100/200/1000 nm of titanium, platinum, and gold respectively. High-energy electrons will go through the electrodes with little interaction ($R_{1\ MeV\ e\text{-}}$ = 402 μm, $R_{15\ MeV\ e\text{-}}$ = 4500 μm, $R_{90\ MeV\ e\text{-}}$ = 9600 μm), thus the decrease in the electron flux reaching the detecting volume due to the electrodes in negligible. When medium-energy x-rays are used as the incident radiation, then the decrease in flux due to the electrodes is not negligible but is easily compensated: in the case of 10 keV or 6 keV x-rays (values found in the next sections), 77% of the 10 keV x-rays will go through 1300 nm of Au (37% for 6 keV x-rays). This attenuation can be compensated by slightly increasing the x-ray flux or energy, or moving the detector closer to the source.

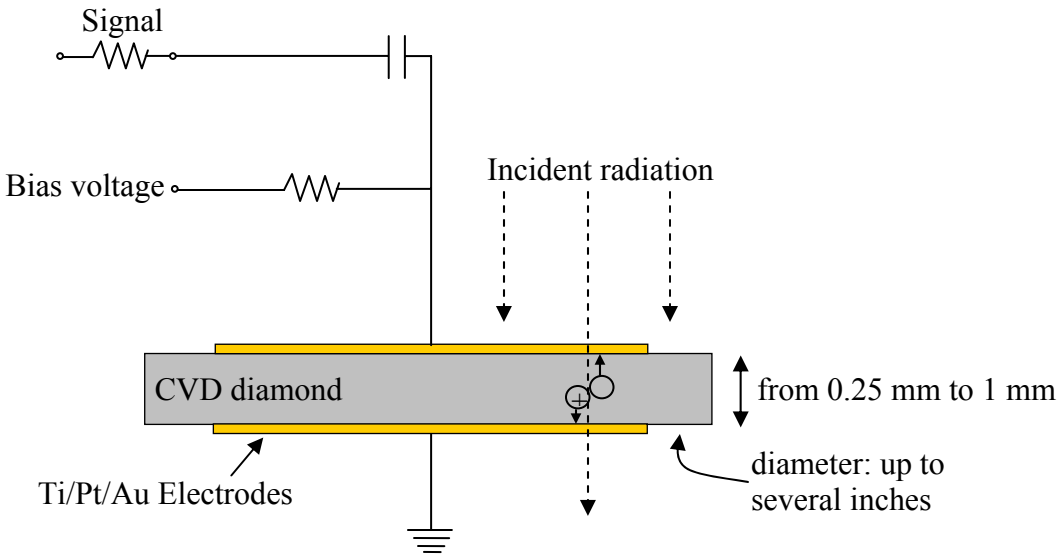

Figure 6: Schematic of a CVD diamond detector with titanium-platinum-gold electrodes coated on both upper and lower surfaces.

C.1. Charge carrier density and signal produced by incident x-rays

To check the feasibility of using x-rays to excite and saturate a CVD diamond wafer to the levels found during a NIF DT implosion, we must calculate the charge carrier density produced in a CVD diamond wafer by a flux of x-rays of varying energies. The signal collected on the electrodes (which is different from that recorded by the oscilloscope since HV and oscilloscope limitations are not included) will also be calculated. If we assume that charged particle equilibrium is true, then the dose deposited, D, in a medium from an incident x-ray flux is equal to:

$$D\left(\frac{J}{g}\right) = \phi_\gamma\left(\frac{\gamma}{cm^2}\right) E_\gamma\left(\frac{eV}{\gamma}\right) 1.6*10^{-19}\left(\frac{J}{eV}\right) \frac{\mu_{en}}{\rho}\left(\frac{cm^2}{g}\right)$$

$$D\left(\frac{J}{g}\right) = 1.6*10^{-19}\ \phi_\gamma\ E_\gamma\ \frac{\mu_{en}}{\rho} \qquad (9)$$

where D is the energy deposited per unit mass (1 Gy =1 J/kg), ϕ_γ is the flux of incident x-rays in x-rays/cm^2, E_γ is the x-ray energy in eV, μ_{en}/ρ is the mass energy-absorption coefficient in cm^2/g (given in Appendix A), and ρ is the density of the medium in g/cm^3.

The energy deposited, E_{dep}, in a wafer of volume V (cm^3) and density ρ can then be deduced from the dose deposited using equation 9.

$$E_{dep}(J) = D\left(\frac{J}{g}\right) \rho\left(\frac{g}{cm^3}\right) V(cm^3)$$

$$E_{dep}(J\ or\ eV) = \phi_\gamma\ E_\gamma(\frac{J\ or\ eV}{\gamma})\ \mu_{en}\ V \quad (10)$$

Using equation 1, we can find the charge carrier density such as:

$$D_{e^-/h^+}(\frac{N_{e^-/h^+}}{cm^3}) = \frac{E_{dep}\ (eV)}{V * \varepsilon_{e^-/h^+}} \quad (11)$$

$$D_{e^-/h^+} = \frac{\phi_\gamma\ E_\gamma\ \mu_{en}}{\varepsilon_{e^-/h^+}} \quad (12)$$

The charge deposited in the detector's volume, Q_{dep}, is given in equation 2. Using equation 6, the collected charge, i.e. measured charge Q_{meas}, is:

$$Q_{meas} = Q_{dep} * \eta \quad (13)$$

The total signal, S, measured on a 50 Ω measuring device is given by the following equations.[1] Once again, the signal recorded on such a measuring device does not include HV and oscilloscope saturations. The maximum value of d is ℓ, and A is the surface of the detector in cm^2.

$$S(V\ ns) = \frac{Q_{meas}(pC)}{20} \quad (14)$$

$$S(V\ ns) = 8*10^{-9}\ D_{e^-/h^+}\ A\ d \quad (15)$$

$$S(V\ ns) = 8*10^{-9}\ \frac{\phi_\gamma\ E_\gamma\ \mu_{en}\ A\ d}{\varepsilon_{e-/h+}} \quad (16)$$

Equation 15 shows that the signal measured is only a function of $D_{e\text{-}h+}$ and d (thus E) for a given detector. Both saturations are included in this equation: saturation due to the decrease in charge carrier mobility attributed to carrier-carrier scattering between electrons and holes (d decreases above 10^{16} e^-h^+/cm^3), and saturation due to the limitation of the applied HV. Indeed, large signals (large $D_{e\text{-}h+}$) will reduce the bias voltage E through the detector, leading to a decrease of the sensitivity and of d. In addition, the maximum height of the signal will saturate at a much lower $D_{e\text{-}h+}$ (thus incident flux) and stay at a constant value equal to that of the high voltage through the wafer, E(V/cm)*ℓ(cm). At the same time, the width of the pulse will increase since it takes a longer time to collect all the charges. This is also true when electrons are used as discussed below.

C.2. Charge carrier density and signal produced by incident electrons

We use the term β for the incident electrons to avoid confusion with the electrons-holes created during ionization of the medium. The following equations are valid if the

incident electrons go through the medium without loosing much of their energy, thus having a constant stopping power. This condition is true in our case since the thickness of a CVD diamond is a few hundreds of micrometers, and the energy of electron beams can be very high, in tens of MeV. The energy lost in collision interactions by an electron flux, ϕ_β, of energy E_β through a thin layer of a medium of volume V, density ρ, and thickness ℓ is given by the following equation:[27]

$$E_{dep}(eV) = 10^6 \left(\frac{eV}{MeV}\right) * \phi_\beta \left(\frac{\beta}{cm^2}\right) * \left.\frac{dE_\beta}{\rho * d\ell}\right|_c \left(\frac{MeV * cm^2}{g * \beta}\right) * \rho \left(\frac{g}{cm^3}\right) \; V(cm^3) \quad (17)$$

where $dE_\beta/(\rho * d\ell)_c$ is the mass collision stopping power of the electrons in the medium (values are given in appendix B). The collision stopping power, $dE_\beta/d\ell_c$, can also be used in equation 16 by multiplying the mass collision stopping power by the density. Using equation 11, the density of charge carrier created in this volume, $D_{e-/h+}$, is found to be:

$$D_{e^-/h^+}\left(\frac{N_{e^-/h^+}}{cm^3}\right) = 10^6 \frac{\phi_\beta \left.\frac{dE_\beta}{d\ell}\right|_c}{\varepsilon_{e^-/h^+}} \quad (18)$$

The signal, S, measured on a 50 Ω measuring device is then given by equation 15 where the charge carrier density is that of equation 18 (the maximum value of d is ℓ):

$$S(V\,ns) = 8 * 10^{-9} \; D_{e^-/h^+} \; A \; d \quad (19)$$

We can now calculate the charge carrier density and the signal produced inside the detector's volume as a function of the flux and energy of the incident x-rays and electrons. As previously mentioned, the signal produced inside the wafer (proportional to the collected charge, Q_{meas}) is different from the oscilloscope signal that can be modified by the limitations due to the applied HV, the detection electronics, and the oscilloscope.

C.3. Charge carrier density and signal produced by a NIF DT implosion

The objective of this work is to study if x-rays or electrons can be used to excite the CVD diamond detector in a way that is similar to that during expected Deuterium-Tritium (DT) implosions at the National Ignition Facility. To do so, $D_{e-/h+}$ produced by x-rays and electrons need to be compared to that produced by 14 MeV DT neutrons at the NIF. In the previous study mentioned in the introduction, the response of a optical grade CVD diamond detector to different NIF DT shots was simulated (figure 1). The integral under the 14 MeV peak, S, and other quantities can be estimated from this plot for both successful and failed ignition. Using the 2D fizzle curve of figure 1 and previous equations, the following quantities can be extracted:

S = 70 V * 6 ns = 420 Vns
Q_{meas} = $2*10^{11}$ * S = 8.4 nC (from equation 14)
Q_{dep} = Q_{meas} / η = 42 nC (from equation 6)
E_{dep} = $\varepsilon_{e\text{-}h+}$* Q_{dep} = $5.6*10^{-7}$ J (from equation 1)
ζ = Q_{meas} / E_{dep} = 0.015 C/J (from equation 5)
ξ = S / $\Phi_{14MeV\ n}$ = 1.05 μVns/n
$D_{e-/h+}$ = Q_{meas} / ($1.6*10^{-19}$ * η *V) = $2.6*10^{12}$ e^-h^+/cm^3 (from equations 2, 6)

The same process is used in the case of the 1D clean burn 14 MeV peak (successful ignition). The results for both DT implosions are given in table 2.

Table 2. Integral under the 14 MeV neutron peak, S, charge collected at the electrodes, Q_{meas}, ionization charge and energy deposited in the detector's volume, Q_{dep} and E_{dep}, sensitivities ξ^1 and ζ, and charge carrier density, $D_{e-/h+}$, for both typical NIF DT implosions. The results are for E = 1 V/μm, ℓ = 1 mm, A = 1 cm^2, optical grade CVD diamond. The charge collection distance is d = 200 μm (at 1V/ μm). The efficiency η of the detector is then 0.2.

	2D fizzle	**1D clean burn**
Y_n (n)	2.10E+16	7.40E+18
ϕ_n (n/cm^2) at L=17m	5.78E+08	2.04E+11
$\phi_{14MeV\ n}$ (n/cm^2) at L=17m	4.00E+08	1.60E+11
S (Vns)	420 (= 4.2E+08 μVns)	1.60E+05 (= 1.6E+11 μVns)
Q_{meas} (nC)	8.4	3200
Q_{dep} (nC)	42	16000
E_{dep}(J)	5.6E-07	2.12E-04
ζ (C/J)	0.015	0.015
ξ (μVns/n) at 14 MeV	1.05	1
D_{e-h+} (e-h+/cm^3)	2.6E+12	1E+15

Sensitivities with two different units are used: ξ is defined in a previous report[1] as the integral under the signal per incident neutron and is in units of μVns/n, ζ is defined by equation 6. Both sensitivities are linked by the following equation:

$$\xi\left(\frac{\mu V\ ns}{n}\right) = 5*10^{16}\left(\frac{\mu V\ ns}{C}\right)\ \zeta\left(\frac{C}{J}\right)\ \frac{E_{dep}}{n}\left(\frac{J}{n}\right) \qquad (20)$$

The values of ζ in table 2 are calculated using equation 5 and correspond to the value given by ζ =d/ (ℓ$\varepsilon_{e\text{-}h+}$). The calculated values of ξ match well the value of 1 that was taken to normalize the ξ curve to 1 μVns/n at 14 MeV.[1] The value of S will scale with the value of ξ, so for instance if ξ = 0.62 μVns/n, then S = $4.2*10^8$ * 0.62 = $2.6*10^8$ μVns. The other quantities of table 2 are then calculated using the new value of S. The same happens when A and d increase, S scales up proportionally.

In addition, we can check that previous experimental data can be found scaling the data of table 2. Previous work found a ξ of 0.62 μVns/n and $1.24*10^{-17}$ C/n (14 MeV) for a 1 cm^2 x 1 mm optical grade CVD polycrystalline diamond, d ≈ 50 μm, at E = 1V/μm, with a 50Ω measuring system.[10,28] Both values of ξ have to be scaled to the data of figure 1: ξ = 1 μVns/n and ξ = $1.24 *10^{-17} /0.62 = 2*10^{-17}$ C/n. For the 2D fizzle case, we can then calculate the expected S and Q_{meas} that we would obtain using the earlier data: $S_{exp} = 1* 4*10^8 = 4*10^8$ μVns and $Q_{meas,exp} = 2*10^{-17} * 4*10^8 = 8$ nC (values close to the ones in table 2). We can also compare the data of table 2 with the integral under the 14 MeV peak found at Omega.[25] In this previous experiment, the signal integral produced by several DT shots in two 10 mm x 1 mm CVD polycrystalline diamonds (thus A = 0.78 cm^2) were recorded. The neutron yields were from 10^{13} to $4.3*10^{13}$ neutrons and the detectors were located at 2.8 m (E = 0.75 V/μm) and 5.4 m (E = -1.5 V/μm). These results were scaled to obtain the signal integral in a detector located at 20 m from the target chamber center, and for higher neutron yields (from 10^{15} to 10^{18} n). These scaled data give S = 250 Vns for a neutron yield of $2*10^{16}$ n corresponding to $4*10^8$ n/cm^2 at 20 m, which is similar to the yield found during a 2D fizzle shot. Scaling this result to 17 m we find S = 346 V ns, and finally taking into account the difference in surface area (0.78 cm^2 in the omega shots compared to 1cm^2 used for the 2D fizzle shot simulation), we obtain S = 440 V ns which is close to the 420 Vns found from figure 1. In conclusion, from the S_{simu} = 420 Vns simulated with ℓ_{simu} = 1 mm, E_{simu} = 1 V/μm, A_{simu} = 1 cm^2, L_{simu} = 17 m, we can infer the value of the measured signal integral for E_{meas} = 0.75 V/μm, A_{meas} = 0.78 cm^2, L_{meas} = 20 m, by doing the following:

$$S_{meas} = S_{simu} * \frac{Y_{n\,meas}}{Y_{n\,simu}} * \left(\frac{L_{simu}}{L_{meas}}\right)^2 * \frac{A_{meas}}{A_{simu}} * \frac{\alpha(E_{meas})}{\alpha(E_{simu})} * \frac{d_{meas}}{d_{simu}} \qquad \text{for } d<\ell \qquad (21)$$

where Y_n is the neutron yield, and the ratio α takes into account the change in charge collection distance d as a function of electric field, which has been measured in previous studies[16,17,23,24,29]:

α (0.50 V/μm) = 0.7 α (1.00 V/μm) = 1 α (1.50 V/μm) = 1.25
α (0.75 V/μm) = 0.85 α (1.25 V/μm) = 1.15

The charge collection distance of the simulated data, d_{simu}, is equal to 0.84 μm, and d_{meas} has to be measured. In the previous example, if we assume that both detectors have a similar charge collection distance, we can infer the signal integral in the 10 mm x 1 mm CVD diamond at a neutron yield equal to $6*10^{15}$ n, and for E = 0.75 V/μm: $S_{meas} = 420 * (6*10^{15}/2.1*10^{16}) * (17/20)^2 * (0.785/1) * (0.85/1) * 1 = 60$ Vns. This is the value found while scaling experimental data from Omega shots.[25]

In the 2D fizzle shot case (failed ignition), $D_{e-/h+}$ is more than 3 orders of magnitude below saturation levels of the CVD diamond wafer, i.e. 10^{16} e^-h^+/cm^3. We can then be confident that even if the parameters previously mentioned vary, the detector wafer will not saturate, and saturation may only come from the surrounding electronics or from the oscilloscope. In the 1D clean burn case (successful ignition), $D_{e-/h+}$ is higher but still does not quite saturate the CVD diamond wafer. Since nuclear diagnostics are

designed primarily for ignition failure recovery, we can assume that the CVD diamond wafer will not saturate in critical NIF ignition experiments.

D. Results and discussion

D.1. Can we use x-rays to excite the CVD diamond to sufficient levels?

In order to use x-rays to excite the CVD diamond wafer at density levels close to these found during the two NIF DT implosions studied, thus from around $2*10^{12}$ to 10^{15} e^-h^+/cm^3 (see table 2), we need to find the energy and flux of x-rays needed to produce such densities. We can expect that it will take high x-ray fluxes to reach these densities since the diamond is very insensitive to photons. Table 3 shows x-ray mass attenuation coefficients for carbon, μ/ρ, ratio of x-ray fluxes $I(x=\ell)/I_0(x=0)$, and absorption depth, $1/\mu$, as a function of x-ray energy.

Table 3. X-ray mass attenuation coefficients for carbon, μ/ρ, ratio of x-ray fluxes $I(x=\ell)/I_0(x=0)$, and absorption depth, $1/\mu$, as a function of x-ray energy.

$E_{x\text{-}ray}$ (keV)	μ/ρ (cm^2/g)	$I/I_0 = e^{-\mu\ell}$ (250 μm)	$I/I_0 = e^{-\mu\ell}$ (1000 μm)	$1/\mu$ (mm)
1	2211.0000			0.0013
1.5	700.2000	1.74E-27		0.0041
2	302.6000	2.72E-12		0.0094
3	90.3300	3.53E-04	1.55E-14	0.0315
4	37.7800	0.0360	1.68E-06	0.0752
5	19.1200	0.1859	0.0012	0.1486
6	**10.9500**	**0.3815**	**0.0212**	**0.2594**
6.5	**9.3565**	**0.4389**	**0.0371**	**0.3036**
7	**7.7630**	**0.5050**	**0.0651**	**0.3660**
8	**4.5760**	**0.6685**	**0.1997**	**0.6208**
10	**2.3730**	**0.8115**	**0.4337**	**1.1972**
15	0.8071	0.9314	0.7527	3.5199
20	0.4420	0.9619	0.8559	6.4274
30	0.2562	0.9777	0.9138	11.0886
40	0.2076	0.9819	0.9295	13.6845
50	0.1871	0.9837	0.9363	15.1839
60	0.1753	0.9847	0.9402	16.2060
80	0.1610	0.9859	0.9449	17.6454
100	0.1514	0.9868	0.9481	18.7643
150	0.1347	0.9882	0.9537	21.0906
200	0.1229	0.9892	0.9577	23.1156
300	0.1066	0.9907	0.9632	26.6502

The minimum x-ray energy necessary is chosen so that the absorption depth of an x-ray at that energy is at least equal to the thickness of the detector. The volume of the detector is then fully excited, with 1/e = 37% of the x-rays going all the way through the wafer. The higher the energy, the larger the absorption depth, thus the more uniform the irradiation. But on the other hand, the higher the incident energy, the lower the energy absorbed in the detector's volume, thus a higher x-ray flux is needed to obtain the same signal. For example, if the thickness is 250 μm, then the minimum $E_{x\text{-}ray}$ necessary for

rough uniform excitation is 6 keV. When ℓ = 1000 μm, then the minimum $E_{x\text{-}ray}$ is 10 keV. Since the thicknesses of available polycrystalline CVD diamond range from 250 to 1000 μm, then we need a minimum $E_{x\text{-}ray}$ between 6 and 10 keV. The maximum $E_{x\text{-}ray}$ will be limited by the x-ray flux required to obtain the necessary charge carrier density.

The previous equations are used to calculate the energy deposited, E_{dep}, the charge carrier density, $D_{e\text{-}/h+}$, the charge created and measured, Q_{dep} and Q_{meas}, the sensitivity of the detector, ζ, and the signal produced, S, as a function of the incident x-ray energy. Table 4 gives these value for a 250 μm * 1 cm^2 polycrystalline CVD diamond, with E = 1 V/μm, so that the $D_{e\text{-}/h+}$ created by a 6 keV flux of x-rays ($1/\mu \approx 250$ μm) corresponds to the 2D fizzle $D_{e\text{-}/h+}$ ($2.6*10^{12}$ e^-h^+/cm^3). The same quantities are given for a 1000 μm * 1 cm^2 polycrystalline CVD diamond in table 5, so that the $D_{e\text{-}/h+}$ created by a 10 keV flux of x-rays ($1/\mu \approx 1000$ μm) corresponds to the 2D fizzle $D_{e\text{-}/h+}$. The charge carrier density is obtained by increasing the incident x-ray flux until the appropriate $D_{e\text{-}/h+}$ is reached. We see that higher energies can be used, but a higher incident x-ray flux is then needed to get the $2.6*10^{12}$ e-h+/cm^3. Since most of the diagnostic interest resides in monitoring ignition failure (2D fizzle), only tables for 2D fizzle shots are shown.

Table 4. Energy deposited, E_{dep} (eV), density of electron/hole pairs created in the detector's volume, $D_{e\text{-}h+}$ (e-h+/cm^3), charge deposited, Q_{dep} (pC) and charge collected, Q_{meas} (pC), sensitivity of the detector, ζ (C/J), and signal integral, S (V ns), as a function of x-ray energy, with ℓ = 250 μm, A = 1 cm^2, and d = 200 μm.

ℓ (μm) =	250		ρ (g/cm^3) =		3.52		
A (cm^2) =	1		x-ray flux (γ/cm^2) =		**1.6E+08**		
E (V/μm)=	1		ε (eV/e-h+) =		13.3		
Energy (keV)	**E_{dep} (ev)**	**$D_{e\text{-}h+}$ (e-h+/cm^3)**	**Q_{dep} (pc)**	**ζ (C/J)**	**Q_{meas} (pC)**	**S (V ns)**	**1/μ**
1	3.11E+13	9.35E+13	3.75E+05	6.02E-02	3.00E+05	1.50E+04	0.0013
1.5	1.48E+13	4.44E+13	1.78E+05	6.02E-02	1.42E+05	7.11E+03	0.0041
2	8.49E+12	2.55E+13	1.02E+05	6.02E-02	8.18E+04	4.09E+03	0.0094
3	3.79E+12	1.14E+13	4.56E+04	6.02E-02	3.65E+04	1.82E+03	0.0315
4	2.10E+12	6.31E+12	2.53E+04	6.02E-02	2.02E+04	1.01E+03	0.0752
5	1.31E+12	3.95E+12	1.58E+04	6.02E-02	1.27E+04	6.33E+02	0.1486
6	**8.90E+11**	**2.68E+12**	**1.07E+04**	**6.02E-02**	**8.58E+03**	**4.29E+02**	**0.2594**
6.5	**8.21E+11**	**2.47E+12**	**9.88E+03**	**6.02E-02**	**7.91E+03**	**3.95E+02**	**0.3036**
7	**7.28E+11**	**2.19E+12**	**8.77E+03**	**6.02E-02**	**7.02E+03**	**3.51E+02**	**0.3660**
8	**4.78E+11**	**1.44E+12**	**5.76E+03**	**6.02E-02**	**4.60E+03**	**2.30E+02**	**0.6208**
10	**2.93E+11**	**8.80E+11**	**3.52E+03**	**6.02E-02**	**2.82E+03**	**1.41E+02**	**1.1972**
15	1.19E+11	3.57E+11	1.43E+03	6.02E-02	1.15E+03	5.73E+01	3.5199
20	6.30E+10	1.90E+11	7.59E+02	6.02E-02	6.07E+02	3.04E+01	6.4274
30	2.79E+10	8.40E+10	3.37E+02	6.02E-02	2.69E+02	1.35E+01	11.0886
40	1.88E+10	5.66E+10	2.27E+02	6.02E-02	1.81E+02	9.07E+00	13.6845
50	1.69E+10	5.08E+10	2.03E+02	6.02E-02	1.63E+02	8.13E+00	15.1839
60	1.77E+10	5.33E+10	2.13E+02	6.02E-02	1.71E+02	8.54E+00	16.2060
80	2.29E+10	6.90E+10	2.76E+02	6.02E-02	2.21E+02	1.11E+01	17.6454
100	3.02E+10	9.09E+10	3.64E+02	6.02E-02	2.91E+02	1.46E+01	18.7643
150	5.17E+10	1.56E+11	6.23E+02	6.02E-02	4.98E+02	2.49E+01	21.0906
200	7.48E+10	2.25E+11	9.01E+02	6.02E-02	7.20E+02	3.60E+01	23.1156
300	1.21E+11	3.65E+11	1.46E+03	6.02E-02	1.17E+03	5.84E+01	26.6502

A minimum incident x-ray flux of $1.6*10^8$ (ℓ=250 μm) and $4.8*10^8$ (ℓ=1000 μm) x-rays/cm^2 is necessary to excite the CVD diamond detector to levels required by a 2D fizzle 14 MeV peak. Consequently, the second peak (mimicking the downscattered neutron signal) requires $1.6*10^5$ (ℓ=250 μm) and $4.8*10^5$ (ℓ=1000 μm) x-rays/cm^2. For a 1D clean burn shot, the required fluxes are $6*10^{10}$ (ℓ=250 μm) and $1.9*10^{11}$ (ℓ=1000 μm) x-rays/cm^2 for the 1st pulse and $6*10^7$ (ℓ=250 μm) and $1.9*10^8$ (ℓ=1000 μm) for the 2nd pulse. Furthermore, this x-ray pulse must be delivered on the surface of the detector in a few nanoseconds. Table 4 and 5 show that the signal integral created when $D_{e-/h+} = 2.6*10^{12}$ e^-h^+/cm^3 is similar to that created by 14 MeV neutrons (2D fizzle shot): S ≈ 425 V ns. This value is equal to that found in table 2.

A few x-ray beam facilities were investigated to see if such high x-ray fluxes are available. Those facilities are:

1. The Advanced Light Source (ALS, Berkeley National Lab.)[30,31]
2. The Stanford Linear Accelerator Center and the Stanford Positron Electron Accelerating Ring (SLAC and SPEAR, Stanford University)[32-34]
3. The National Synchrotron Light Source (NSLS, Brookhaven National Lab.)[35-37]
4. The Advanced Photon Source (APS, Argonne National Lab.)[37,38]
5. The Janus laser (Lawrence Livermore National Lab.)[39,40]

Table 5. Same as table 4 for a detector's thickness ℓ = 1000 μm.

ℓ (μm) =	1000		ρ (g/cm^3) =		3.52		
A (cm^2) =	1		x-ray flux (γ/cm^2) =		4.8E+08		
E (V/μm)=	1		ε (eV/e-h+) =		13.3		
Energy (keV)	E_{dep} (ev)	D_{e-h+} (e-h+/cm^3)	Q_{dep} (pc)	ζ (C/J)	Q_{meas} (pC)	S (V ns)	1/μ
1	3.73E+14	2.81E+14	4.50E+06	1.50E-02	8.99E+05	4.50E+04	0.0013
1.5	1.77E+14	1.33E+14	2.13E+06	1.50E-02	4.27E+05	2.13E+04	0.0041
2	1.02E+14	7.66E+13	1.23E+06	1.50E-02	2.46E+05	1.23E+04	0.0094
3	4.54E+13	3.42E+13	5.47E+05	1.50E-02	1.09E+05	5.47E+03	0.0315
4	2.52E+13	1.89E+13	3.03E+05	1.50E-02	6.06E+04	3.03E+03	0.0752
5	1.58E+13	1.19E+13	1.90E+05	1.50E-02	3.80E+04	1.90E+03	0.1486
6	**1.07E+13**	**8.03E+12**	**1.29E+05**	**1.50E-02**	**2.57E+04**	**1.29E+03**	**0.2594**
6.5	**9.85E+12**	**7.40E+12**	**1.19E+05**	**1.50E-02**	**2.37E+04**	**1.19E+03**	**0.3036**
7	**8.74E+12**	**6.57E+12**	**1.05E+05**	**1.50E-02**	**2.11E+04**	**1.05E+03**	**0.3660**
8	**5.73E+12**	**4.31E+12**	**6.91E+04**	**1.50E-02**	**1.38E+04**	**6.91E+02**	**0.6208**
10	**3.51E+12**	**2.64E+12**	**4.23E+04**	**1.50E-02**	**8.46E+03**	**4.23E+02**	**1.1972**
15	1.43E+12	1.07E+12	1.72E+04	1.50E-02	3.44E+03	1.72E+02	3.5199
20	7.56E+11	5.69E+11	9.11E+03	1.50E-02	1.82E+03	9.11E+01	6.4274
30	3.35E+11	2.52E+11	4.04E+03	1.50E-02	8.08E+02	4.04E+01	11.0886
40	2.26E+11	1.70E+11	2.72E+03	1.50E-02	5.44E+02	2.72E+01	13.6845
50	2.02E+11	1.52E+11	2.44E+03	1.50E-02	4.88E+02	2.44E+01	15.1839
60	2.13E+11	1.60E+11	2.56E+03	1.50E-02	5.12E+02	2.56E+01	16.2060
80	2.75E+11	2.07E+11	3.32E+03	1.50E-02	6.63E+02	3.32E+01	17.6454
100	3.63E+11	2.73E+11	4.37E+03	1.50E-02	8.74E+02	4.37E+01	18.7643
150	6.21E+11	4.67E+11	7.48E+03	1.50E-02	1.50E+03	7.48E+01	21.0906
200	8.97E+11	6.75E+11	1.08E+04	1.50E-02	2.16E+03	1.08E+02	23.1156
300	1.45E+12	1.09E+12	1.75E+04	1.50E-02	3.50E+03	1.75E+02	26.6502

None of the cyclotrons/synchrotrons (1) through (3) are bright enough. The maximum monoenergetic x-ray flux available at the energies of interest (6-10 keV) is about 10^4 x-rays/ns/mrad (0.1% band), equal to about 10^4 x-rays/ns/cm^2 at 10 m from the source. The maximum white beam x-ray flux (thus all energies of x-rays are used) is about 10^6 x-rays/ns/mrad, equal to 10^6 x-rays/ns/cm^2 at 10 m from the source. Those numbers are well below the over 10^8 (2D fizzle shot) or 10^{11} (1D clean burn shot) x-rays/cm^2 necessary. Also, obtaining double pulses separated from 50 to 300 ns seems very challenging due to the continuous nature of the x-ray beam.[31,34,37] The factor of 1000 contrast between the 1st and 2nd pulse may also be very difficult to achieve.[34]

Another synchrotron, the APS (4), has higher fluxes, but the numbers listed for their facility are still too low.[38] Beam time at this facility is also difficult to obtain. Finally, the Janus laser-based x-rays facility (5) may be able to generate the experimental conditions we need.[40] The x-ray flux generated by the laser photons hitting a nickel or zinc target is large enough, with over 10^{11} x-rays/cm^2 produced at 10 cm from the target (7.5 keV to 8.6 keV x-rays lines).[41] Double pulses can be obtained as well. However, the fluctuations in the laser intensity may be a limitation to obtain a uniform x-ray flux at the detector. Also the monitoring and filtering (to absorb low-energy x-rays) of the x-ray spectrum reaching the detector may be challenging.

D.2. Can we use electrons to excite the CVD diamond to sufficient levels?

By looking at the upper graph of appendix B, we can see that a minimum energy of 300 keV (or 800 keV) is required in order to get an electron range of the order of the detector thickness, 250 μm (or 1000 μm). Also, the second graph in appendix B shows that increasing E_β beyond about 800 keV will not increase $dE_\beta/(d\ell)_c$, thus that will not increase $D_{e\text{-}h+}$. Increasing $D_{e\text{-}h+}$ will then rely on increasing the charge per shot. This is verified in table 6 where electron flux, mass collision stopping power, $dE_\beta/(\rho*d\ell)_c$, collision stopping power, $dE_\beta/(d\ell)_c$, and charge carrier density, $D_{e\text{-}h+}$, are calculated for different electron energies and charge per shot.

For the minimum energy of 300 keV or above, the required 1D clean burn $D_{e\text{-}h+}$ (10^{15} e-h+/cm^3) is reached for about 400 pC/shot, and the 2D fizzle $D_{e\text{-}h+}$ ($2.6*10^{12}$ e-h+/cm^3) requires about 1 pC/shot. The linac facility at LLNL can produce 5 pC to 100 pC double pulses, with electron energies ranging from 15 to 90 MeV. Therefore, for a 100 pC beam (any energy), the 1D clean burn $D_{e\text{-}h+}$ cannot be quite achieved, but the 2D fizzle $D_{e\text{-}h+}$ is easily reached with the lower setting of 5 pC/shot. The characteristics of x-ray or electron pulses needed for the double pulse experiment that would mimic the 1D clean burn and the 2D fizzle NIF DT implosions are given in figure 7. The electron flux needed to simulate the 2D fizzle downscattered signal is low and requires about 1 fC/shot beam. This may be done at the LLNL linac by collimating or filtering the beam to reach lower intensities than the current minimum of 5 pC. Other linac facilities have higher currents and can reach the 10^{15} e-h+/cm^3 required for the 1D clean burn, as well as lower currents to reach 1fC/shot., but obtaining a double pulse may be challenging. In conclusion, the linac facilities at LLNL can answer the requirements needed to simulate

both the 14 MeV peak and the downscattered neutron signal of a 2D fizzle shot, and are a factor of 3 below the densities required in the the 1D clean burn case.

Table 6. Electron flux, collision stopping power, $dE_\beta/(d\ell)_c$ and charge carrier density, $D_{e\text{-}h+}$ as a function of the energy of the incident electrons, E_β, and the charge in each electron pulse, Q_{dep}.

	Q_{dep}		MeV cm^2/g β	MeV/cm β	
E_β (MeV)	pC/shot	β flux (β/cm^2)	$(dE/\rho d\ell)_c$	$(dE/d\ell)_c$	$D_{e\text{-}h+}$ (e-h+/cm^3)
0.1	1	6.24E+06	3.647	12.84	6.03E+12
	5	3.12E+07			3.01E+13
	200	1.25E+09			1.21E+15
	400	2.50E+09			2.41E+15
	1000	6.24E+09			6.03E+15
0.3	1	6.24E+06	2.065	7.27	3.41E+12
	5	3.12E+07			1.71E+13
	200	1.25E+09			6.82E+14
	400	2.50E+09			1.36E+15
	1000	6.24E+09			3.41E+15
0.8	1	6.24E+06	1.625	5.72	2.68E+12
	5	3.12E+07			1.34E+13
	200	1.25E+09			5.37E+14
	400	2.50E+09			1.07E+15
	1000	6.24E+09			2.68E+15
15	1	6.24E+06	1.741	6.13	2.88E+12
	5	3.12E+07			1.44E+13
	200	1.25E+09			5.75E+14
	400	2.50E+09			1.15E+15
	1000	6.24E+09			2.88E+15
90	1	6.24E+06	1.886	6.64	3.12E+12
	5	3.12E+07			1.56E+13
	200	1.25E+09			6.23E+14
	400	2.50E+09			1.25E+15
	1000	6.24E+09			3.12E+15

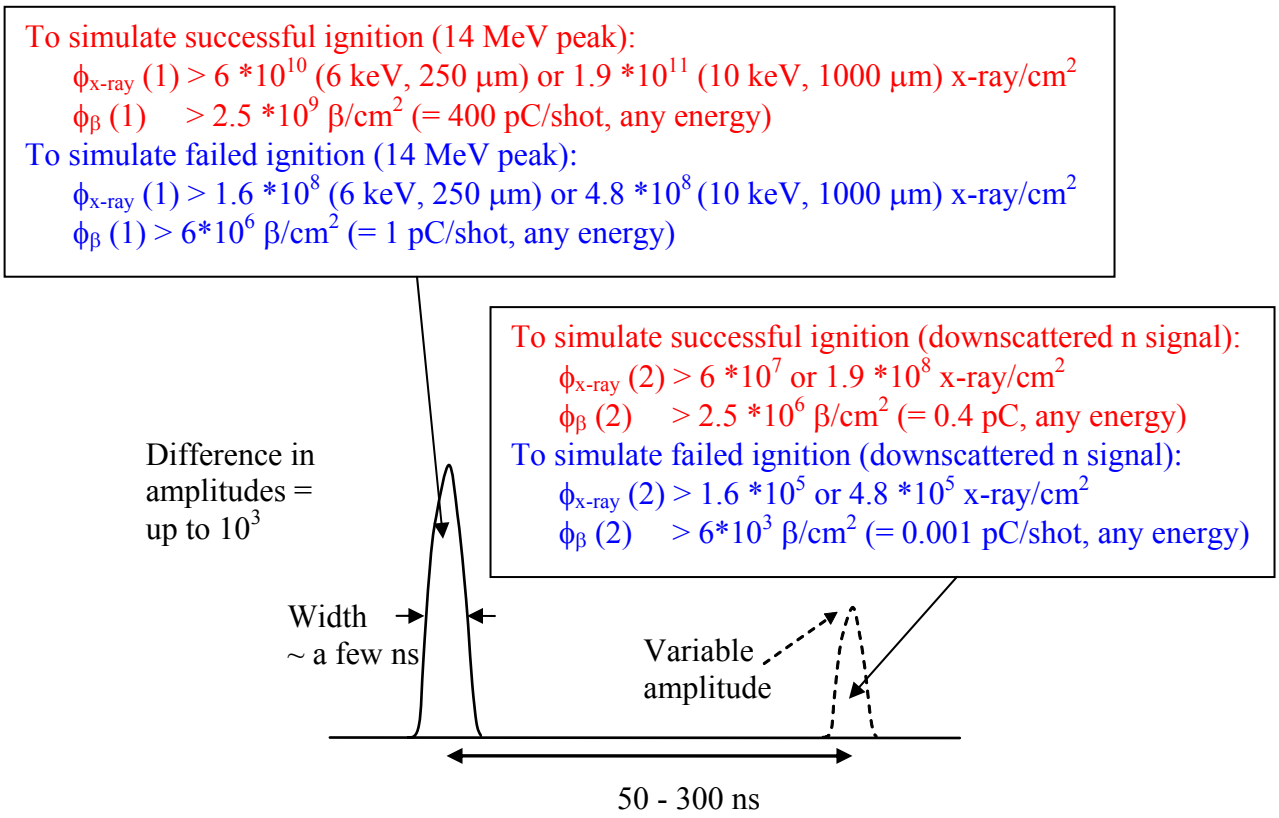

*Figure 7. Double x-ray pulses with the necessary x-ray and electron fluxes to create 10^{15} e-h+/cm^3 (successful ignition) or 2.6*10^{12} e-h+/cm^3 (failed ignition) in the 1st pulse.*

Conclusion

For both failed and successful ignitions at the NIF, the diamond wafer will not saturate due to an excessive number of charge carriers produced. When the detector is placed at 17 m from the target chamber center, densities of charge carriers stay below 10^{16} e^-h^+/cm^3, value at which recombination of the electrons and holes become a significant process due to carrier-carrier scattering. For shorter distances from the target, care should be taken to stay below that limit. In addition, the results found in this work are for a 250 μm to 1000 μm x 1cm^2 detector, an typical electric field of 1V/μm, a charge collection distance of 200 μm, a detector to target distance of 17 m (L). They must be scaled up and down if a different A, E, d, or L is used. Other sources of saturation may affect the signals read on the oscilloscope, such as limitations from biasing electronics and from the oscilloscope. The double pulse experiment being planned will quantify these limitations to study the recovery of the CVD diamond detection system after a large pulse. The effect of such a large signal on a weaker signal produced later in time is needed to characterize the impact of the 14 MeV neutron peak on the downscattered neutron signal during NIF ignition attempts. We found that 2.5*10^{12} e^-h^+/cm^3 (typical failed ignition) and 10^{15} e^-h^+/cm^3 (successful ignition) are produced in the 14 MeV

neutron peak. Since high-flux neutron sources capable of producing such densities are not available, the experiments must use other sources of radiation such as x-rays or electrons.

We have demonstrated that, for a CVD diamond detector thickness of 250 μm to 1000 μm, 6 keV to 10 keV x-rays are needed to fully excite the detector's volume. The x-ray fluxes required to obtain the charge carrier density of the 14 MeV peak during a failed ignition are $1.6*10^8$ x-rays/cm^2 (250 μm) and $4.8*10^8$ x-rays/cm^2 (1000 μm). The fluxes necessary for the second pulse (mimicking the downscattered neutron signal) are 1000 times lower. For successful ignition, x-ray fluxes must be up to $6*10^{10}$ x-rays/cm^2 (250 μm) and $1.9*10^{11}$ x-rays/cm^2 (1000 μm) for the large pulse, and 1000 times lower for the second pulse. Such high fluxes, delivered in nanoseconds and with the possibility of producing double pulses, are not available at cyclotrons/synchrotrons, but are available at the Janus laser facility at the Lawrence Livermore National Laboratory (10^{11} x-rays/cm^2 at 10 cm from a zinc or nickel target, 7.5 - 8.6 keV lines). However, implementation of the experiments at Janus will be challenging largely because of the non-uniformity of the x-ray flux emitted from the target, the monitoring of the x-ray spectrum incident on the detector, and the filtering of the low-energy x-rays.

For the same range of detector's thicknesses, a minimum electron energy of 300 keV to 800 keV is required to fully excite the detector's volume. Above 800 keV, the charge carrier density is mostly independent of the electron energy, thus the following fluxes are obtained for electrons with energies from 800 keV to about 1000 MeV. An electron flux of $6*10^6$ β/cm^2 (≈ 1 pC/shot) is necessary to obtain the charge carrier density of the 14 MeV peak during a failed ignition, and $6*10^3$ β/cm^2 (≈ 0.001 pC/shot) for the second pulse. The LLNL linac can produce double pulses with sufficient fluxes to obtain failed ignition charge carrier densities, since each pulse can have from 5 pC to 100 pC. The second pulse requires a lower intensity (0.001 pC) than the minimum available intensity (5 pC). Collimating or filtering the electron beam will reduce this intensity but may be challenging because the monitoring of this collimated or filtered beam will be difficult. Also, the ability to obtain a contrast of 1000 between the heights of both pulses needs to be experimentally demonstrated. For a successful ignition, the minimum flux required goes up to $2.5*10^9$ β/cm^2 (≈ 400 pC/shot) for the large pulse, and $2.5*10^6$ β/cm^2 (≈ 0.4 pC/shot) for the second pulse. The LLNL linac cannot quite produce the large pulse (successful ignition) since it has a maximum of 100 pC per shot. However, monitoring failed ignitions at the NIF is the main goal of the CVD diamond detectors, thus obtaining charge carrier densities slightly below that found during a successful ignition is acceptable. Other linac facilities have a larger dynamic range in pC/shot and could produce electron fluxes low and high enough. Nevertheless, producing double pulses may be a challenge.

Acknowledgements

We would like to thank Nobuhiko Izumi and Dick Lerche for their assistance, Joe McDonald, Franz Weber, Eddy Dewald, Kelly Campbell, and Andy Mackinnon for their kind advice.

References

[1]L. Dauffy, R. Lerche, and T. Phillips, "*Response of a CVD diamond detector to typical Deuterium-Tritium NIF implosions for areal density measurement*", Lawrence Livermore National Laboratory, Report No. UCRL-TR-211523, 2005.

[2]L. Dauffy, R. Lerche, G. Schmid, and J. Koch, "*Study of the saturation of CVD diamond detectors using laser pulses*", Lawrence Livermore National Laboratory, Report No. UCRL unpublished, 2005.

[3]E. Souw, R. Meilunas, C. Szeles, N. Ravindra, and F. Tong, "*Photoconductivity of CVD diamond under bandgap and subbandgap irradiations*", DIAM RELAT MATER **6**, 1157-1171 (1997).

[4]C. Nebel, "*Electronic properties of CVD diamond*", SEMICOND SCI TECH **18**, S1-S11 (2003).

[5]G. Knoll, in "*Radiation Detection and Measurement*", (John Wiley & Sons, Inc., New York),Chap. 11, pp. p365.(1999).

[6]E. Nappi, "*Charged Particle Identification via Ionization Energy Loss and Time-of-Flight Measurements*", ICFA lecture, Morelia, Italy, 2004.

[7]G. Lutz, in "*Semiconductor Radiation Detectors*", (Springer, New-York),Chap. 4, pp. 91.(1999).

[8]D. Kania, M. Landstrass, M. Plano, L. Pan, and S. Han, "*Diamond Radiation Detectors*", DIAM RELAT MATER **2**, 1012-1019 (1993).

[9]H. Pernegger, S. Roe, P. Weilhammer, V. Eremin, H. Frais-Kolbl, E. Griesmayer, H. Kagan, S. Schnetzer, R. Stone, W. Trischuk, D. Twitchen, and A. Whitehead, "*Charge-carrier properties in synthetic single-crystal diamond measured with the transient-current technique*", J APPL PHYS **97**, - (2005).

[10]G. Schmid, R. Griffith, N. Izumi, J. Koch, R. Lerche, M. Moran, T. Phillips, R. Turner, V. Glebov, T. Sangster, and C. Stoeckl, "*CVD diamond as a high bandwidth neutron detector for inertial confinement fusion diagnostics*", REVIEW OF SCIENTIFIC INSTRUMENTS **74**, 1828-1831 (2003).

[11]J. Kaneko, T. Tanaka, T. Imai, Y. Tanimura, M. Katagiri, T. Nishitani, H. Takeuchi, T. Sawamura, and T. Iida, "*Radiation detector made of a diamond single crystal grown by a chemical vapor deposition method*", NUCL INSTRUM METH A **505**, 187-190 (2003).

[12]R. Alig and S. Bloom, "*Electron-Hole-Pair Creation Energies In Semiconductors*", PHYS REV LETT **35**, 1522-1525 (1975).

[13]Ortec, "Creation of Electron-Hole Pairs in Semiconductor Detectors by Ionizing Radiation -http://www.ortec-online.com/detectors/review_physics/creation.htm," (2005).

[14]R. Tapper, "*Diamond detectors in particle physics*", REP PROG PHYS **63**, 1273-1316 (2000).

[15]G. Schmid, J. Koch, R. Lerche, and M. Moran, "*A neutron sensor based on single crystal CVD diamond*", NUCL INSTRUM METH A **527**, 554-561 (2004).

[16]L. Pan, S. Han, D. Kania, S. Zhao, K. Gan, H. Kagan, R. Kass, R. Malchow, F. Morrow, W. Palmer, C. White, S. Kim, F. Sannes, S. Schnetzer, R. Stone, G. Thomson, Y. Sugimoto, A. Fry, S. Kanda, S. Olsen, M. Franklin, J. Ager, and P. Pianetta, "*Particle-Induced and Photoinduced Conductivity in Type-IIA diamonds*", J APPL PHYS **74**, 1086-1095 (1993).

[17]L. Pan, S. Han, D. Kania, M. Plano, and M. Landstrass, "*Electrical-Properties Of High-Quality Diamond Films*", DIAM RELAT MATER **2**, 820-824 (1993).
[18]L. Pan, D. Kania, P. Pianetta, and O. Landen, "*Carrier Density dependent Photoconductivity in Diamond*", APPL PHYS LETT **57**, 623-625 (1990).
[19]C. Manfredotti, "*CVD diamond detectors for nuclear and dosimetric applications*", DIAM RELAT MATER **14**, 531-540 (2005).
[20]J. Isberg, J. Hammersberg, H. Bernhoff, D. Twitchen, and A. Whitehead, "*Charge collection distance measurements in single and polycrystalline CVD diamond*", DIAM RELAT MATER **13**, 872-875 (2004).
[21]G. Conte, M. Rossi, S. Salvatori, P. Ascarelli, and D. Trucchi, "*Thin polycrystalline diamond for low-energy x-ray detection*", J APPL PHYS **96**, 6415-6420 (2004).
[22]J. Isberg, J. Hammersberg, E. Johansson, T. Wikstrom, D. Twitchen, A. Whitehead, S. Coe, and G. Scarsbrook, "*High carrier mobility in single-crystal plasma-deposited diamond*", SCIENCE **297**, 1670-1672 (2002).
[23]M. Marinelli, E. Milani, A. Paoletti, A. Tucciarone, G. Rinati, M. Angelone, and M. Pillon, "*High collection efficiency in chemical vapor deposited diamond particle detectors*", DIAM RELAT MATER **9**, 998-1002 (2000).
[24]C. Jany, A. Tardieu, A. Gicquel, P. Bergonzo, and F. Foulon, "*Influence of the growth parameters on the electrical properties of thin polycrystalline CVD diamond films*", DIAM RELAT MATER **9**, 1086-1090 (2000).
[25]V. Glebov, "*Progress with CVD diamond detector for ICF Neutron Time-of-Flight (NToF) applications*", presented at the International Conference On Plasma Science, Monterey, California, 2005 (unpublished).
[26]M. Fraser, Harris International,"*Size of polycrystalline CVD diamond crystals* ". Private communication. 2005.
[27]F. Attix, in "*Introduction to radiological physics and radiation dosimetry*", (Wiley-Interscience, New-York), pp. 187.(1986).
[28]G. Schmid, V. Glebov, A. Friensehner, D. Hargrove, S. Hatchett, N. Izumi, R. Lerche, T. Phillips, T. Sangster, C. Sibernagel, and C. Stoeckl, "*CVD diamond detectors for current mode neutron time-of-flight spectroscopy at OMEGA/NIF*", Charged Particle Detection, Diagnostics, and Imaging **4510**, 12-19 (2001).
[29]T. Behnke, P. Huntemeyer, A. Oh, J. Steuerer, A. Wagner, and W. Zeuner, "*The charge collection properties of CVD diamond*", NUCL INSTRUM METH A **414**, 340-356 (1998).
[30]"*Advance Ligth Source, ALS, Berkeley National Laboratory*", http://www-als.lbl.gov/als/. (2005).
[31]N. Smith, "*X-ray beam parameters at the Advanced Light Source (Berkeley National Lab.)*". Private communication. 2005.
[32]"*The Stanford Linear Accelerator Center, SLAC, Stanford University.*" http://www.slac.stanford.edu/. (2005).
[33]"*The Stanford Positron Electron Accelerating Ring, SPEAR, Stanford University*", http://www2.slac.stanford.edu/vvc/experiments/spear.html. (2005).
[34]P. Pianetta, "*X-ray beam parameters at the Stanford Linear Accelerator Center (Stanford University).*" Private communication. 2005.
[35]"*The National Synchrotron Light Source, NSLS, Brookhaven National Lab.*" http://www.nsls.bnl.gov/. (2005).

[36]K. Campbell, "*X-ray beam parameters at the National Synchrotron Light Source, NSLS (Brookhaven National Lab.)* ", (2005).
[37]F. Weber, "*X-ray beam parameters at the National Synchrotron Light Source, NSLS (Brookhaven National Lab.)* ". Private communication. 2005.
[38]"*The Advanced Photon Source, APS, Argonne National Lab.* " http://www.aps.anl.gov/. (2005).
[39]"*The Janus laser, Lawrence Livermore National Lab.*" http://www.llnl.gov/str/Springer2.html. (2005).
[40]A. MacKinnon, "*Laser and X-ray beam characteristics at the Janus facility, Lawrence Livermore National Lab.*" Private communication. 2005.
[41]D. Matthews, E. Campbell, N. Ceglio, G. Hermes, R. Kauffman, L. Koppel, R. Lee, K. Manes, V. Rupert, V. Slivinsky, R. Turner, and F. Ze, "*Characteristic of laser-produced plasma x-ray sources for use in x-ray radiography*", J APPL PHYS **54**, 4260-4268 (1983).

Appendix A: X-ray mass attenuation coefficients for Carbon, μ/ρ and μ_{en}/ρ (NIST)

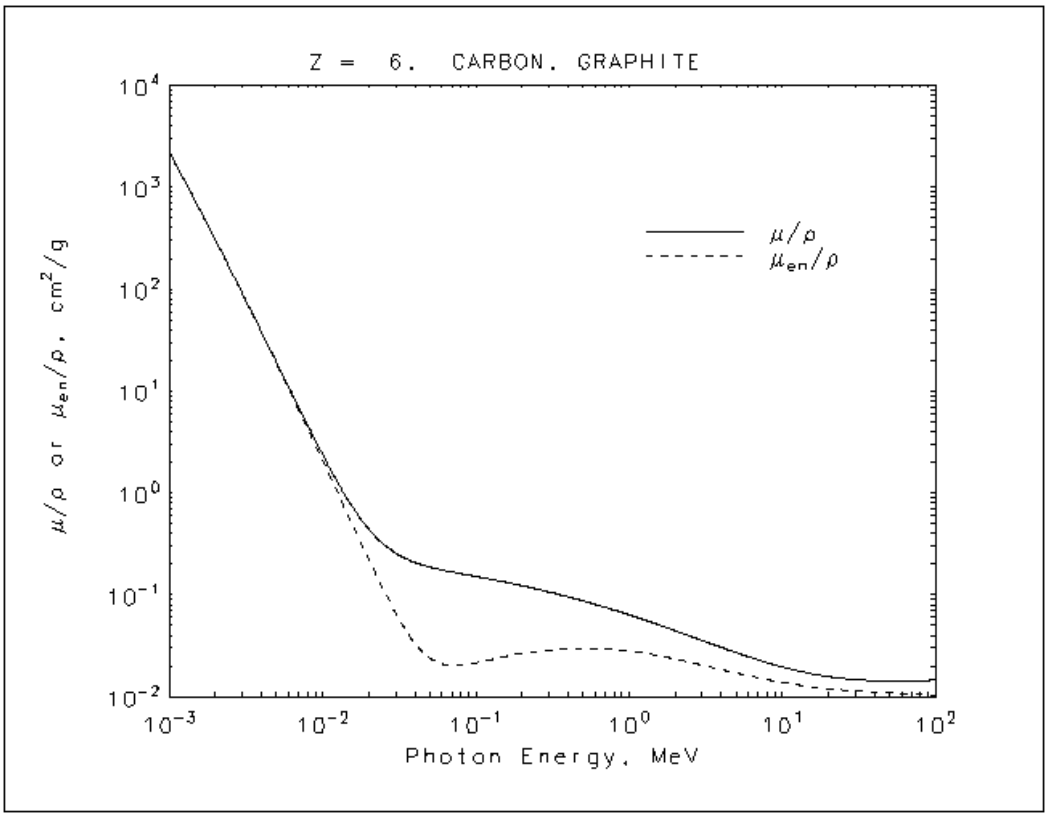

Energy (MeV)	μ/ρ (cm²/g)	μ_{en}/ρ (cm²/g)
1.00000E-03	2.211E+03	2.209E+03
1.50000E-03	7.002E+02	6.990E+02
2.00000E-03	3.026E+02	3.016E+02
3.00000E-03	9.033E+01	8.963E+01
4.00000E-03	3.778E+01	3.723E+01
5.00000E-03	1.912E+01	1.866E+01
6.00000E-03	**1.095E+01**	**1.054E+01**
8.00000E-03	**4.576E+00**	**4.242E+00**
1.00000E-02	**2.373E+00**	**2.078E+00**
1.50000E-02	8.071E-01	5.627E-01
2.00000E-02	4.420E-01	2.238E-01
3.00000E-02	2.562E-01	6.614E-02
4.00000E-02	2.076E-01	3.343E-02
5.00000E-02	1.871E-01	2.397E-02
6.00000E-02	1.753E-01	2.098E-02
8.00000E-02	1.610E-01	2.037E-02
1.00000E-01	1.514E-01	2.147E-02
1.50000E-01	1.347E-01	2.449E-02
2.00000E-01	1.229E-01	2.655E-02
3.00000E-01	1.066E-01	2.870E-02
4.00000E-01	9.546E-02	2.950E-02
5.00000E-01	8.715E-02	2.969E-02
6.00000E-01	8.058E-02	2.956E-02
8.00000E-01	7.076E-02	2.885E-02
1.00000E+00	6.361E-02	2.792E-02
1.25000E+00	5.690E-02	2.669E-02
1.50000E+00	5.179E-02	2.551E-02
2.00000E+00	4.442E-02	2.345E-02
3.00000E+00	3.562E-02	2.048E-02
4.00000E+00	3.047E-02	1.849E-02
5.00000E+00	2.708E-02	1.710E-02
6.00000E+00	2.469E-02	1.607E-02
8.00000E+00	2.154E-02	1.468E-02
1.00000E+01	1.959E-02	1.380E-02
1.50000E+01	1.698E-02	1.258E-02
2.00000E+01	1.575E-02	1.198E-02

Appendix B: Electron stopping power and ranges in CVD diamond (ESTAR NIST)

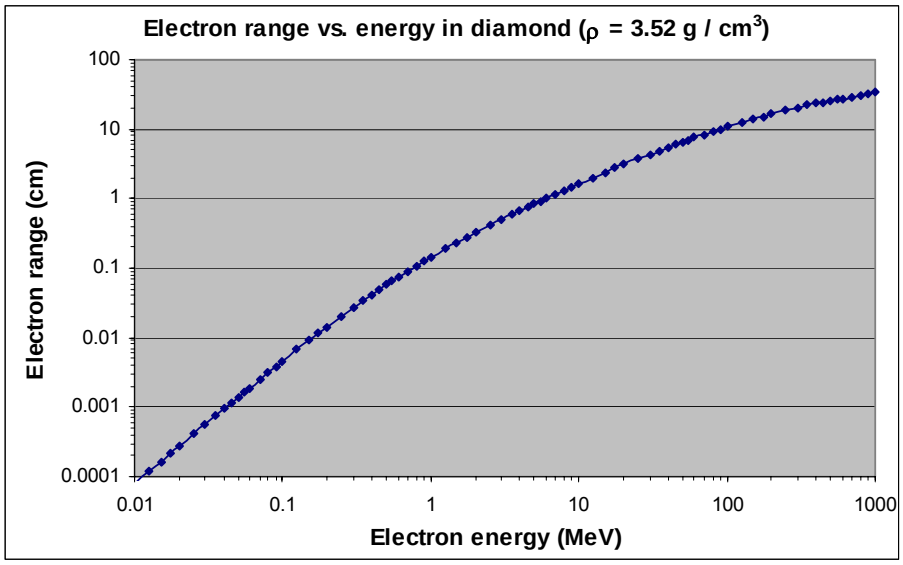

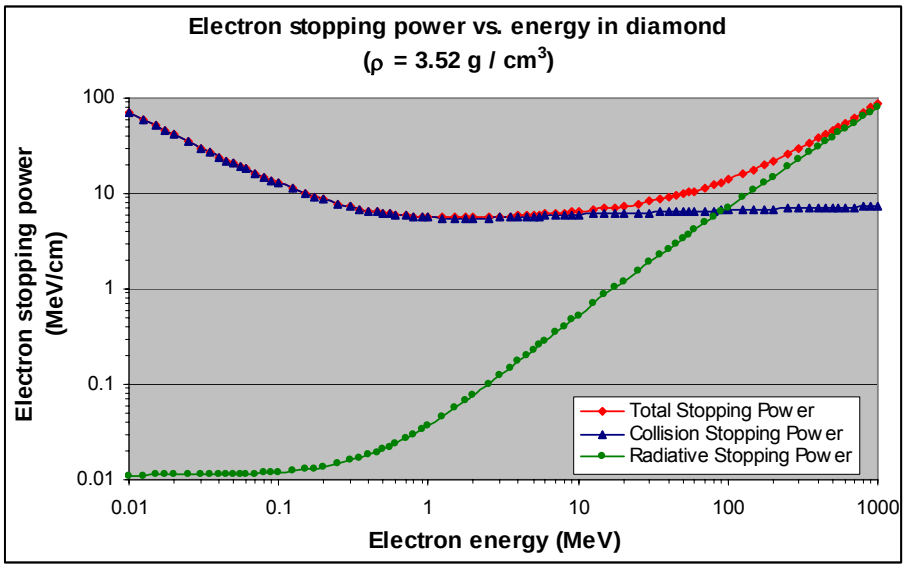

ESTAR: Stopping Powers and Range Tables for Electrons
CVD Diamond (Density = 3.52 g/cm3) (I = 81.0 eV)

Kinetic Energy MeV	Collision Stp. Pow. MeV cm2/g	Radiative Stp. Pow. MeV cm2/g	Total Stp. Pow. MeV cm2/g	CSDA Range g/cm2
1.000E-02	1.998E+01	3.150E-03	1.999E+01	2.845E-04
2.000E-02	1.169E+01	3.176E-03	1.169E+01	9.670E-04
3.000E-02	8.567E+00	3.194E-03	8.570E+00	1.981E-03
4.000E-02	6.903E+00	3.215E-03	6.906E+00	3.291E-03
5.000E-02	5.861E+00	3.241E-03	5.864E+00	4.869E-03
6.000E-02	5.144E+00	3.270E-03	5.147E+00	6.695E-03
7.000E-02	4.620E+00	3.303E-03	4.623E+00	8.749E-03
8.000E-02	4.219E+00	3.337E-03	4.223E+00	1.102E-02

9.000E-02	3.903E+00	3.375E-03	3.906E+00	1.348E-02
1.000E-01	3.647E+00	3.414E-03	3.650E+00	1.613E-02
1.500E-01	2.863E+00	3.640E-03	2.866E+00	3.179E-02
2.000E-01	2.463E+00	3.896E-03	2.467E+00	5.071E-02
3.000E-01	2.065E+00	4.489E-03	2.069E+00	9.546E-02
4.000E-01	1.873E+00	5.173E-03	1.878E+00	1.464E-01
5.000E-01	1.765E+00	5.935E-03	1.771E+00	2.014E-01
6.000E-01	1.698E+00	6.759E-03	1.705E+00	2.590E-01
7.000E-01	1.654E+00	7.637E-03	1.662E+00	3.185E-01
8.000E-01	1.625E+00	8.559E-03	1.633E+00	3.792E-01
9.000E-01	1.605E+00	9.523E-03	1.614E+00	4.408E-01
1.000E+00	1.591E+00	1.053E-02	1.601E+00	5.030E-01
1.500E+00	1.565E+00	1.602E-02	1.581E+00	8.181E-01
2.000E+00	1.568E+00	2.213E-02	1.590E+00	1.134E+00
2.500E+00	1.579E+00	2.870E-02	1.607E+00	1.446E+00
3.000E+00	1.591E+00	3.561E-02	1.627E+00	1.756E+00
3.500E+00	1.603E+00	4.281E-02	1.646E+00	2.061E+00
4.000E+00	1.615E+00	5.026E-02	1.665E+00	2.363E+00
4.500E+00	1.626E+00	5.792E-02	1.684E+00	2.662E+00
5.000E+00	1.636E+00	6.576E-02	1.702E+00	2.957E+00
5.500E+00	1.645E+00	7.378E-02	1.719E+00	3.249E+00
6.000E+00	1.654E+00	8.193E-02	1.736E+00	3.539E+00
7.000E+00	1.669E+00	9.865E-02	1.768E+00	4.110E+00
8.000E+00	1.682E+00	1.158E-01	1.798E+00	4.671E+00
9.000E+00	1.694E+00	1.334E-01	1.827E+00	5.222E+00
1.000E+01	1.704E+00	1.513E-01	1.855E+00	5.765E+00
1.500E+01	1.741E+00	2.444E-01	1.985E+00	8.369E+00
2.000E+01	1.766E+00	3.417E-01	2.108E+00	1.081E+01
2.500E+01	1.785E+00	4.417E-01	2.226E+00	1.312E+01
3.000E+01	1.800E+00	5.435E-01	2.343E+00	1.531E+01
3.500E+01	1.812E+00	6.466E-01	2.459E+00	1.739E+01
4.000E+01	1.823E+00	7.508E-01	2.573E+00	1.938E+01
4.500E+01	1.832E+00	8.559E-01	2.688E+00	2.128E+01
5.000E+01	1.840E+00	9.617E-01	2.802E+00	2.310E+01
5.500E+01	1.848E+00	1.068E+00	2.916E+00	2.485E+01
6.000E+01	1.855E+00	1.175E+00	3.030E+00	2.653E+01
7.000E+01	1.867E+00	1.391E+00	3.258E+00	2.972E+01
8.000E+01	1.877E+00	1.608E+00	3.485E+00	3.268E+01
9.000E+01	1.886E+00	1.827E+00	3.713E+00	3.546E+01
1.000E+02	1.894E+00	2.046E+00	3.940E+00	3.808E+01
1.250E+02	1.912E+00	2.598E+00	4.510E+00	4.400E+01
1.500E+02	1.926E+00	3.155E+00	5.081E+00	4.922E+01
1.750E+02	1.938E+00	3.714E+00	5.652E+00	5.388E+01
2.000E+02	1.948E+00	4.276E+00	6.224E+00	5.810E+01
2.500E+02	1.965E+00	5.405E+00	7.371E+00	6.547E+01
3.000E+02	1.979E+00	6.540E+00	8.519E+00	7.178E+01
3.500E+02	1.991E+00	7.678E+00	9.669E+00	7.728E+01
4.000E+02	2.001E+00	8.820E+00	1.082E+01	8.217E+01
4.500E+02	2.010E+00	9.964E+00	1.197E+01	8.656E+01
5.000E+02	2.019E+00	1.111E+01	1.313E+01	9.054E+01
5.500E+02	2.026E+00	1.226E+01	1.428E+01	9.419E+01
6.000E+02	2.033E+00	1.340E+01	1.544E+01	9.756E+01
7.000E+02	2.044E+00	1.570E+01	1.775E+01	1.036E+02
8.000E+02	2.055E+00	1.801E+01	2.006E+01	1.089E+02
9.000E+02	2.064E+00	2.031E+01	2.238E+01	1.136E+02
1.000E+03	2.072E+00	2.262E+01	2.469E+01	1.179E+02